

# A Modified Exact Reconstruction Algorithm to Determine the Complex Permittivity Perturbations of a Cancer-Affected Biological Target Using the Microwave Tomography Technique

Deborsi Basu<sup>†</sup> and Kabita Purkait, Non-members

## ABSTRACT

As an emerging technology, the microwave tomography technique (MTT) is demonstrating its effectiveness in detecting cancer at an early stage. Due to the random, non-deterministic characteristics of cancer cells, more advancements are required in MTT to accurately detect the presence and location of the affected region. In this paper, we consider this fundamental issue and propose a modified exact reconstruction algorithm (mERA) capable of providing a detailed analysis of all kinds of complex dielectric perturbations in any cancer-affected biological target. In MTT, the detection of a cancerous tumor inside any organ of the human body is performed using different image reconstruction algorithms. In contrast, the proposed algorithm in this study uses a selective data segregation mechanism to generate the perturbed complex cell permittivity of the affected organ tissues. The efficiency of our approach in detecting all types of dielectric variations such as large (20%), small (5%), positive or negative has also been verified, even in a mixed scenario where affected cells possess all types of perturbations simultaneously. As a cancerous cell shows peculiar behavior inside the human body and its nature varies from person to person and even in between the different stages (1, 2, 3, and 4) of cancer, the algorithm is designed in such a way that it can detect the presence of a tumor taking all these possibilities into account. The results validate the high accuracy and effectiveness of the proposed mERA in the field of cancer diagnosis.

**Keywords:** Modified Exact Reconstruction Algorithm, mERA, Cancerous Tumor, Complex Dielectric

Manuscript received on June 7, 2020 ; revised on December 12, 2020 ; accepted on April 10, 2021. This paper was recommended by Associate Editor Suramate Chalermwisutkul.

The authors are with the Department of Electronics and Communication Engineering, Kalyani Government Engineering College, Kalyani, Nadia, West Bengal, India

<sup>†</sup>Corresponding author: deborsibasus2015@gmail.com

©2021 Author(s). This work is licensed under a Creative Commons Attribution-NonCommercial-NoDerivs 4.0 License. To view a copy of this license visit: <https://creativecommons.org/licenses/by-nc-nd/4.0/>.

Digital Object Identifier 10.37936/ecti-ec.2021193.244937

Permittivity, Dielectric Perturbations, Microwave Tomographic Technique, MTT

## 1. INTRODUCTION

Microwave tomography is currently showing some remarkable results in different areas of biomedicine [1,2], specifically the detection of cancerous tumors inside the human body. The MTT can detect the presence of tumors based on certain cell properties and is considered to be one of the best among the existing techniques such as X-ray computed tomography, MR imaging (MRI), positron emission, ultrasound, C-ray imaging, etc. [3,4].

The devastation caused by cancer is increasing every year across the globe. Global fatalities due to cancer reached almost 10 million in 2020 [5]. In the next five years, the global parameter of cancer-affected people is expected to pass the 50-million mark by the end of 2021. This increasing rate of casualties is driving researchers to think deeply to develop effective methods for early diagnosis. The cancer mortality rate can be curbed if the cases can be detected and treated at the early phase [6]. MTT is a helpful diagnostic tool to detect cancer at an early stage when used with a proper reconstruction algorithm and the appropriate methodology. To date, different image reconstruction algorithms have been used in MTT such as the 3-D image reconstruction algorithm based on the forward difference time domain (FDTD) algorithm [7,8], the 2D point-spread-function-based iterative reconstruction algorithm [9], an inverse iterative algorithm for microwave imaging based on the method of moments [10], etc. All these techniques have their own accuracy and error minimization criteria. The proper algorithm is selected based on the specific situation. Apart from cancer cell detection, reconstruction algorithms are also applied in brain stroke detection along with some changes to the fundamental frequency of operation and antenna radiation pattern [11,12]. Among the various biomedical applications, creating a suitable algorithm that is effective in all possible cases remains a challenging issue and researchers are rigorously working to find a solution, especially in the case

of cancerous cell detection. It is important that a suitable algorithm is created with the ability to detect cancer from the initial to the critical stage. Considering the increasing demand for the MTT in cancerous cell detection, this work also attempts to develop a new algorithmic approach to aid future cancer diagnosis.

In this work, a new approach is proposed to improve the existing reconstruction algorithms. The advanced simultaneous iterative reconstruction algorithm (SIRT) is primarily based on the method of moments [13, 14]. The technique is used mainly to detect dielectric perturbations in the affected bone regions. A modified version of the algorithm is developed in [15, 16] and termed as an improved exact reconstruction algorithm (iERA). This improved version of the algorithm has now been further improved and used here with newly defined concepts. The latest form of the algorithm is known as the modified exact reconstruction algorithm (mERA). All possible perturbations of the complex dielectrics of a cancer-affected cell have been studied using this algorithm. The output results of the reconstructed dielectric constant values reveal that this algorithm can identify all types of variations with minimum errors and produce optimum outcomes.

The remaining portions of the paper are organized as follows. Section 2 details the complex dielectric properties of human tissues. Section 3 describes the experimental model and setup formation. Section 4 elaborates on the mERA derivation. Section 5 explains the processing of the model inside the experimental setup. Section 6 presents an analysis of the detailed output results in a tabular fashion to provide all the possible outcomes of a cancer-affected cell. Section 7 evaluates the output results. Finally, Sections 8 and 9 summarize this work and offer suggestions for its potential future extension.

## 2. LITERATURE REVIEW

Larson and Jacobi were the first to use MTT in biomedical applications during the late 1970s [17, 18], whereby a water-immersed antenna was formed to scan biological targets. The impedance matching of the water medium and human body in this technique helped to penetrate the biological target using a microwave to create images of the internal structures. Through these results, a new path was carved in microwave imaging for biomedical applications [19]. Since the dielectric properties of biological tissues depend on temperature, they are suitable for hyperthermia treatment [20]. Semenov *et al.* [21] attempt to identify other methods of treatment. For example, in the field of breast cancer detection, Meaney *et al.* [22, 23] were the first to employ MTT. Recently, many other groups have also been working in this area of application [24]. The two most common approaches to microwave imaging today are

tomographic and radar. The tomographic approach involves the generation of cross-sectional slices of dielectric properties, while the radar technique is used to find strong scatterers inside an object.

The non-linear deterministic approach was first introduced by Joachimowicz and Chew at the beginning of the 1990s [25]. Caorosi also made an early contribution to this domain [26]. The method is based on the iterative optimization of an objective function using a Newton-based or conjugate gradient-based scheme. The non-linear inverse problem in microwave imaging has attracted the interest of many groups [27, 28]. Since the algorithm is computational heavy, two-dimensional (2D) imaging has mainly been used, although some efforts have been made to initiate the three-dimensional (3D) case. Infinity approximation of the coupling medium is also used for computational saving, whereby the interaction between the antennas, surrounding cover, and object is ignored. This approximation is very useful as long as the background medium is lossy, like water. However, antenna interaction has been implemented in some cases.

Alternative optimizing schemes have recently been reported, such as the multiplicative regularization contrast source inversion by Hopfer *et al.* [29], global optimization using neural networks, genetic algorithms, and non-destructive evaluation by Goetzke-Pala *et al.* [30]. These methods avoid local minima, albeit at the cost of a slower convergence and higher computational load. Until now single frequency solutions have been widely used, but different groups are working on multi-frequency solutions. Low frequencies are known to reduce the effect of phase non-linearities and stabilize the algorithm, while higher frequencies increase the resolution, and the idea is that a combination will improve the reconstruction. However, the frequency dependence of biological tissues is one of the difficulties in this approach and potential future research efforts could focus on this area.

The application of MTT in biomedical image processing using the iterative moment method was performed by Richmond *et al.* [13]. Since then, the same process has been used by many researchers with different antenna orientations and medium constraints [31]. The results are satisfactory, motivating us to apply this fundamental approach with a modified algorithm to validate all the cases of cancer-affected tissues inside the human body. Few test cases have previously been conducted [32] and in this study we have tried to consider all the possible cases of dielectric perturbation in cancer-affected cells inside the human body. The random deviations and abnormal dielectric fluctuations are difficult to monitor in cancerous cells and also vary from person to person. This algorithm mitigates such difficulties and produces a generalized solution based

on all cases. The results are also satisfactory while error levels support the application of this algorithm in biomedical diagnostics. The following sections elaborate on the specific aspects in detail.

### 3. COMPLEX DIELECTRIC PROPERTIES OF HUMAN BODY TISSUES

Scientists and researchers have found it necessary to analyze the behavior of complex dielectric permittivity in the water content inside human body tissues and cells. Based on the variations of the mobile ions inside the water content, the interactive nature between the electromagnetic waves and cell changes altering the field inside it [33,34]. The materialistic dielectric properties are obtained from their respective complex relative permittivity as expressed in the following equation:

$$\varepsilon^* = \varepsilon' - j\varepsilon'' \quad (1)$$

where  $\varepsilon'$  is the relative permittivity of the material and  $\varepsilon''$  is the out-of-phase loss factor associated with it, such that the following equation holds true.

$$\varepsilon'' = \frac{\sigma}{\varepsilon_0 \omega} \quad (2)$$

where  $\sigma$  is the total conductivity of the material. Depending on the nature of the test sample, that may include a contribution from frequency-independent ionic conductivity,  $\varepsilon_0$  is the permittivity of free space and  $\omega$  the angular frequency of the field [35].

The complex dielectric constant value of a normal cell generally follows limited fluctuation with respect to its standard value. On the other hand, cancer-affected cells show significant perturbations in their dielectric values. This phenomenon is known as the capacitance relaxation of cancer cells inside the human body.

#### 3.1 Capacitance relaxation phenomenon in cancer cells

Capacitors are composed of two metallic plates, separated by a dielectric medium. The ability of the system to store the charge is known as capacitance. The fundamental dependency of the capacitance on the medium dielectric is represented by Eq. (3).

$$C = \frac{\varepsilon A}{d} \quad (3)$$

where  $C$  is the capacitance of the medium,  $\varepsilon$  represents the absolute permittivity of the dielectric medium,  $A$  and  $d$  are the area and thickness of the plates and medium, respectively. From Eq. (3), it can clearly be observed that the capacitance and medium dielectric are related and changes in one are reflected in the other.

Inside a cell, the membrane works as a dielectric medium and the charged ions of various minerals

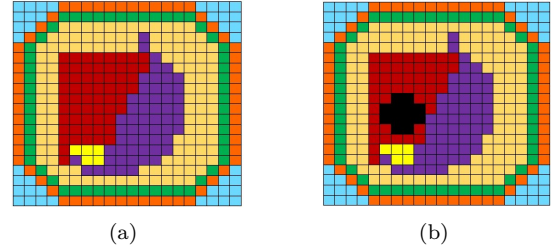


**Fig. 1:** The approximated cross section of a human body model, (a) normal condition and (b) affected condition in the liver region.

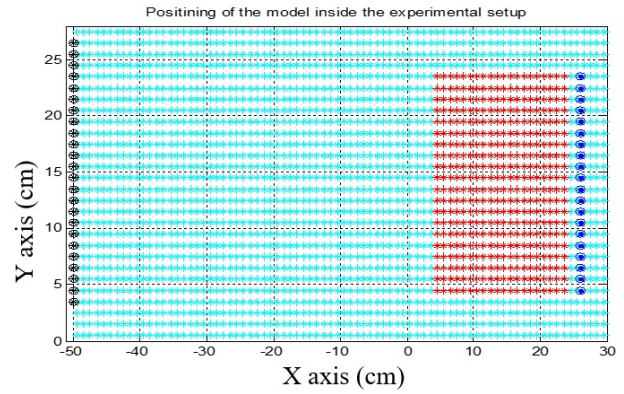


**Fig. 2:** Placement of the experimental model inside the setup.








work as the parallel conductive plates on its two sides. Whenever a cell is affected by cancer, the ionic distribution changes abruptly, and the cell membrane spreads abnormally. This results in a changing dielectric inside the affected region. Furthermore, the electromagnetic fields inside the cell vary when placed inside a proper experimental setup. The relaxation of the cell capacitance then occurs so that it deviates in any direction and in any quantity. This incident is known as the capacitance relaxation phenomenon [36,37]. A reduction in the storage charge capacity is caused by dielectric relaxation [38,39] under the dynamic random-access memory-operating system (RAM-OS).

### 4. FORMATION OF THE EXPERIMENTAL MODEL

The experimental model (as shown in Fig. 1) was placed inside the matching medium (saline water in this case). The distance between the transmitter section to the model was fixed at 50 cm. In Fig. 2, the black dotted lines refer to the 24 transmitter positions. A quarter-wave dipole array antenna with a dimension of  $15 \times 15$  cm was used as a transmitter.

The orientation and positioning of the antenna can be adjusted depending upon the scanning requirements of the target model. The complex dielectric permittivities of different cells of the target model in

**Table 1:** Descriptions of different cell regions (healthy condition).

Region Specification	Name of the Region	No. of Cells Present	Complex Permittivity
	Fat Region	60	$25 - j5$
	Muscle Region	56	$50 - j23$
	Muscle Type Region	123	$35 - j15$
	Liver Region	60	$46 - j10$
	Stomach Region	57	$60 - j18$
	Pancreas Region	5	$65 - j30$
	Matching Medium	40	$76 - j40$

normal conditions (healthy conditions) are mentioned in Table 1.

The receivers are placed inside the matching medium at the end of the model. Twenty such positions are allocated to receive antennas. The blue dotted regions shown in Fig. 2 depict the receiver positions. A halfwave dipole antenna is used as a single receiver. The electromagnetic waves come from the transmitter section, and after passing through the model the scattered waves are received at the receiving end. The entire experiment is conducted inside the matching medium to retain an operational wavelength comparable with the cell dimensions. The receiver section is also flexible and can be adjusted based on the requirements. The accuracy level can be improved by scanning multiple data for the model from different orientations and positions. Finally, an average dataset has been considered and used inside the algorithm to generate the approximated output. One important fact is that the model and receiving section have been placed in the near field region of the transmitting antenna.

## 5. MODEFIED EXACT RECONSTRUCTION ALGORITHM

In microwave tomography, although the concept of geometrical ray tracing fails for biomedical image processing, it is suitable for geo-tomographic cases. One of the primary reasons is the difference in the objective dimension target. The frequency range of the microwave falls under the range at which it complements the biological cells. Moreover, the presence of matching medium results in the complementary matching of the wave nature with the cell membrane. The biomedical image resolutions are in millimeters which is only a fraction of the fundamental wavelength propagated in the medium. The resultant field is calculated considering the cumulative effect of the cells along the ray paths as well as the cells contained within the beamwidth of

the radiation pattern. The optimal effects of the rays are considered in calculating the results. It is assumed that the scattering energy dissipation is controlled by the Tx-Rx sections as per the requirement.

The resultant field induced inside an inhomogeneous biological medium can be calculated using the method of moments in the solution developed by Richmond [13]. The method considers an inhomogeneous dielectric cylinder placed along the  $z$ -axis of the reference frame, illuminated by an electromagnetic wave. As a result, only the  $z$ -component of the field will be maintained. The transverse coordinates (i.e.  $\varepsilon = \varepsilon(x, y)$ ) are used to express the permittivity of the medium. The difference between the total electric field ( $E$ ) incident source in the presence of the dielectric cylinder and the incident field ( $E^i$ ) in the absence of the cylinder is the effective scattered field ( $E^s$ ).

$$E^s = E - E^i. \quad (4)$$

A large number of small cells over the dielectric cylinder helps to distribute a uniform field across the cells. The system of linear equations can be represented in matrix form as in Eq. (5).

$$[C] \cdot [E] = [E^i] \quad (5)$$

where  $[C]$  is the co-efficient matrix corresponding to the fundamental homogeneous medium considered here.  $[E]$  is the total internal field in different cells of the homogeneous medium and  $[E^i]$  is the incident field matrix with different pixels in a vacuum.

Eq. (6) represents the set of linear equations in a compact form.

$$\sum_{n=1}^N C_{mn} E_n = E_m^i \quad \forall m = 1, 2, \dots, N \quad (6)$$

where

$$C_{mn} = (\varepsilon_m - 1) \left( \frac{j}{2} \right) \left[ \pi k a_m H_1^{(2)}(k a_m) - 2j \right] \text{ if } n = m,$$

and

$$C_{mn} = \left( j \pi k \frac{a_n}{2} \right) (\varepsilon_1 - 1) \left[ J_1(k a_n) H_0^{(2)}(k \rho_{mn}) \right] \text{ if } n \neq m.$$

The analogical circular section similar to the cross-sectional area in cells  $n$  and  $m$  have a circular radius of  $a_n$  and  $a_m$ , respectively.  $H_0^{(2)}$  is the Hankel function of type two and order zero, while  $J_1$  is a Bessel function.

The resultant field at the center of each cell is used to solve these  $N$  equations. The cumulative electric field at different receiver locations is calculated to identify different transmitter locations in the microwave tomography imaging process.

After considering each cell in the cylinder, it is assumed that the scattered field represents the summation of the contribution from each of the  $N$  of cells. Although the perturbation method is evaluated using various approaches [41,42], the received field has been processed in order to produce tomographic images.

The complex permittivity of the cells is perturbed due to the presence of inhomogeneous biological cells which are affected by cancer. The small amount of dielectric perturbation  $\Delta\epsilon_i$  ( $i = 1, 2, \dots, n$ ) further changes the internal field by  $\Delta E_i$ . The modified Eq. (5) can now be written as:

$$[C^l] \cdot [E + \Delta E] = [E^i] \quad (7)$$

where  $[C^l]$  is the co-efficient matrix corresponding to the inhomogeneous medium. According to the exact algorithm [13,36], the change in the electric field of different cells is obtained by subtracting Eq. (5) from Eq. (7) and given by

$$\Delta E_i = -x_i E_i^l + \sum x_j E_j^l \frac{M_{ji}(0)}{\Delta(0)} \quad (8)$$

where  $E_i^l = E_i + \Delta E_i$  is the modified field in the  $i^{\text{th}}$  cell under perturbed conditions.  $\Delta(0)$  and  $M_j^i(0)$  are the determinant and cofactor of  $j^{\text{th}}$  and  $i^{\text{th}}$  element of unperturbed co-efficient matrix  $[C]$  respectively.

Let  $E_{Rml}(k)$  denotes the scattered field at the  $l^{\text{th}}$  receiver location for the  $k^{\text{th}}$  beam in the numerical model and  $E_{Rol}(k)$  denotes the calculated scattered field intensity at the same receiver location for the same beam with an assumed uniform baseline permittivity for the object. Therefore, the total change in the scattered field at the  $l^{\text{th}}$  receiver position corresponding to  $k^{\text{th}}$  beam is

$$E_{Rml} - E_{Rol}(k) = \sum_{i=1}^n x_i \sum_{j=1}^n E_j^l \frac{M_{ji}(0)}{\Delta(0)}. \quad (9)$$

The values of  $x_i$ , i.e, the requisite fractional changes in permittivity values for different cells from the assumed initial permittivity for the medium can be determined from the above equation.

### 5.1 Algorithm Based on Method I

In this work, we have proposed the modified exact reconstruction algorithmic approach where the standard normal complex dielectric permittivity values are taken as the initial condition at the start of every iteration.

In order to detect the affected region at an early stage, this type of test case has been prepared for rapid convergence and quick results. The required values of  $x_i^1$  from the corresponding normal values are obtained by Eq. (10).

$$x_i^1 = \frac{\epsilon_{ical} - \epsilon_{inor}}{\epsilon_{inor} - 1} \quad (10)$$

where  $\epsilon_{ical}$  is the complex permittivity of  $i^{\text{th}}$  cell calculated from  $x_i$  and obtained from Eq. (10) using  $E_{i,nor} = E_i^1$ . Internal fields are modified each time by Eq. (8).

### 5.2 Algorithm Based on Method II

Method I detects the approximate affected region inside the experimental model. Another iteration is then made only inside the affected region previously identified by Method I.

The accuracy level of Method II is very high and it is able to detect the exact location of affected regions and the corresponding stages of cancer. The main reason for this high level of accuracy is that the iteration is performed only inside the affected region, leaving the remaining area unaffected.

## 6. PROCESSING OF THE MODEL IN DIFFERENT CONDITIONS USING AN ALGORITHMC APPROACH

In this section, the processing of the experimental model is explained as an input of the experimental setup.

The intermediate processor along with the transceiver system performs the required analysis following the modified reconstruction algorithm and generates the output results. An analysis of the detailed results are shown in flow chart format in Fig. 3.

### 6.1 Data Analysis with Positive Complex Dielectric Perturbations

In this section, the analysis is performed based on small perturbation variations in the complex dielectric constant of the cells belonging to the affected region. The deviation is greater (positive deviation) than that of the normal cell.

The liver region with a standard normal dielectric of  $46 - j10$  is considered to be affected. Detailed analysis of the complex dielectric before and after reconstruction are shown in Tables 2–8. The errors found in the fifth column have been calculated using the error calculation formula in Eq. (11),

$$\text{Error (\%)} = \left| \frac{\text{Complex dielectric in diseased condition}}{\text{Complex dielectric in diseased condition}} \right| \times 100 \quad (11)$$

where the error signifies the deviation of the affected complex dielectric value with respect to that in a healthy cell condition.

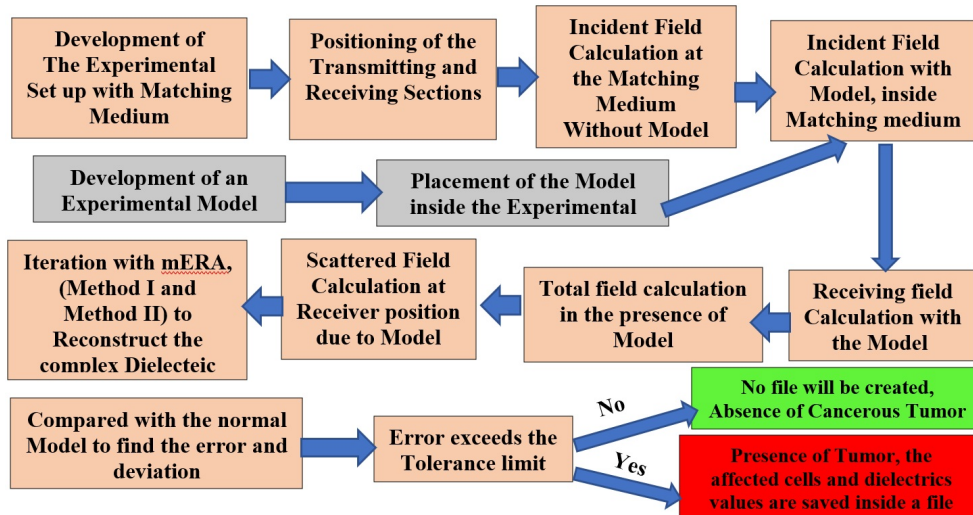


**Fig. 3:** The algorithmic flowchart for mERA.

**Table 2:** Analysis of the reconstructed dielectrics and corresponding errors for the diseased model (5% perturbation) using Method I.

Different organs of the model	Complex dielectric in normal condition	Complex dielectric in diseased condition	Reconstructed complex dielectric with the proposed algorithm	Error found in the reconstructed values (%)
Fat	$25 - j5$	$25 - j5$	$25.02588 - j5.05244$	0.1400
Muscle	$50 - j23$	$50 - j23$	$49.87674 - j22.88554$	0.2903
Muscle Type	$35 - j15$	$35 - j15$	$34.92036 - j15.07454$	0.1147
Pancreas	$65 - j30$	$65 - j30$	$64.91367 - j30.00112$	0.1088
<b>Liver</b>	$46 - j10$	$48.3 - j10.5$	$48.25634 - j10.50991$	4.9289
Stomach	$60 - j18$	$60 - j18$	$59.96296 - j17.99522$	0.0588
Water	$76 - j40$	$76 - j40$	$76 - j40$	0.0000

**Table 3:** Analysis of the reconstructed dielectrics and corresponding errors for the diseased model (10% perturbation) using Method I.

Different organs of the model	Complex dielectric in normal condition	Complex dielectric in diseased condition	Reconstructed complex dielectric with the proposed algorithm	Error found in the reconstructed values (%)
Fat	$25 - j5$	$25 - j5$	$24.95391 - j4.57078$	0.4943
Muscle	$50 - j23$	$50 - j23$	$49.95723 - j22.76435$	0.2488
Muscle Type	$35 - j15$	$35 - j15$	$35.08332 - j14.94211$	0.1414
Pancreas	$65 - j30$	$65 - j30$	$65.24102 - j30.54123$	0.6240
<b>Liver</b>	$46 - j10$	$50.6 - j11$	$50.34289 - j10.90528$	9.4235
Stomach	$60 - j18$	$60 - j18$	$59.42091 - j17.82558$	0.9654
Water	$76 - j40$	$76 - j40$	$76 - j40$	0.0000

**Table 4:** Analysis of the reconstructed dielectrics and corresponding errors for the diseased model (15% perturbation) using Method I.

Different organs of the model	Complex dielectric in normal condition	Complex dielectric in diseased condition	Reconstructed complex dielectric with the proposed algorithm	Error found in the reconstructed values (%)
Fat	$25 - j5$	$25 - j5$	$24.73079 - j5.73967$	0.4196
Muscle	$50 - j23$	$50 - j23$	$49.60423 - j22.58049$	0.9710
Muscle Type	$35 - j15$	$35 - j15$	$34.71792 - j15.14485$	0.5289
Pancreas	$65 - j30$	$65 - j30$	$64.74480 - j30.01244$	0.3162
<b>Liver</b>	$46 - j10$	$52.9 - j11.5$	$52.78141 - j11.55418$	14.7783
Stomach	$60 - j18$	$60 - j18$	$59.91796 - j18.02007$	0.1162
Water	$76 - j40$	$76 - j40$	$76 - j40$	0.0000



**Table 5:** Analysis of the reconstructed dielectrics and corresponding errors for the diseased model (20% perturbation) using Method I.

Different organs of the model	Complex dielectric in normal condition	Complex dielectric in diseased condition	Reconstructed complex dielectric with the proposed algorithm	Error found in the reconstructed values (%)
Fat	$25 - j5$	$25 - j5$	$24.89319 - j4.19063$	0.9870
Muscle	$50 - j23$	$50 - j23$	$49.84424 - j22.52381$	0.6164
Muscle Type	$35 - j15$	$35 - j15$	$35.14381 - j14.86586$	0.2094
Pancreas	$65 - j30$	$65 - j30$	$64.55645 - j28.02348$	1.7230
<b>Liver</b>	$46 - j10$	$55.2 - j12$	$54.67350 - j11.77476$	18.8056
Stomach	$60 - j18$	$60 - j18$	$59.00829 - j17.63408$	1.6841
Water	$76 - j40$	$76 - j40$	$76 - j40$	0.0000

**Table 6:** Analysis of the reconstructed dielectrics and corresponding errors for the diseased model (mixed perturbation) using Method I.

Different organs of the model	Complex dielectric in normal condition	Complex dielectric in diseased condition	Reconstructed complex dielectric with the proposed algorithm	Error found in the reconstructed values (%)
Fat	$25 - j5$	$25 - j5$	$23.85823 - j6.77213$	2.7234
Muscle	$50 - j23$	$50 - j23$	$48.11037 - j22.83154$	3.2402
Muscle Type	$35 - j15$	$35 - j15$	$33.24918 - j15.15035$	4.0459
Pancreas	$65 - j30$	$65 - j30$	$63.43673 - j31.28860$	1.1954
<b>Liver</b>	$46 - j10$	$48.3 - j10.5$	$48.25634 - j10.50991$	4.9289
		$50.4 - j11$	$50.34289 - j10.90528$	9.4235
		$52.9 - j11.5$	$52.78141 - j11.55418$	14.7783
		$55.2 - j12$	$54.67350 - j11.77476$	18.8056
Stomach	$60 - j18$	$60 - j18$	$57.11947 - j19.44377$	3.6775
Water	$76 - j40$	$76 - j40$	$76 - j40$	0.0000

**Table 7:** Analysis of the reconstructed dielectrics and corresponding errors for the diseased model (mixed perturbation) using Method II.

Different organs of the model	Complex dielectric in normal condition	Complex dielectric in diseased condition	Reconstructed complex dielectric with the proposed algorithm	Error found in the reconstructed values (%)
<b>Liver</b>	$46 - j10$	$48.3 - j10.5$	$48.30001 - j10.50014$	5.0001
		$50.4 - j11$	$50.40002 - j10.99999$	10.0004
		$52.9 - j11.5$	$52.89999 - j11.50001$	15.0000
		$55.2 - j12$	$55.20001 - j11.99999$	20.0000

**Table 8:** Comparison between the errors found using Method I and II in the affected liver region.

Different organs of the model	Complex dielectric in normal condition	Complex dielectric in diseased condition	Error found in the reconstructed values (%) using Method I	Error found in the reconstructed values (%) using Method II
<b>Liver</b>	$46 - j10$	$48.3 - j10.5$	4.9289	5.0001
		$50.4 - j11$	9.4235	10.0004
		$52.9 - j11.5$	14.7783	15.0000
		$55.2 - j12$	18.8056	20.0000

## 6.2 Data Analysis with Negative Perturbations of the Complex Dielectric

In similarity to the previous section, here the analysis has also been extended to the perturbations

in the negative direction. The complex dielectric of the cancer-affected region shows a decrease from the standard normal value. (Tables 9–15)

**Table 9:** Analysis with negative perturbations of the reconstructed dielectrics and corresponding errors for the diseased model (5% perturbation) using Method I.

Different organs of the model	Complex dielectric in normal condition	Complex dielectric in diseased condition	Reconstructed complex dielectric with the proposed algorithm	Error found in the reconstructed values (%)
Fat	$25 - j5$	$25 - j5$	$25.02786 - j4.91221$	0.0402
Muscle	$50 - j23$	$50 - j23$	$50.06727 - j22.96679$	0.0858
Muscle Type	$35 - j15$	$35 - j15$	$35.17583 - j15.11028$	0.5385
Pancreas	$65 - j30$	$65 - j30$	$65.08768 - j30.00189$	0.1123
<b>Liver</b>	$46 - j10$	$43.7 - j9.5$	$43.74286 - j9.49063$	4.9319
Stomach	$60 - j18$	$60 - j18$	$60.05104 - j18.01591$	0.0853
Water	$76 - j40$	$76 - j40$	$76 - j40$	0.0000

**Table 10:** Analysis with negative perturbations of the reconstructed dielectrics and corresponding errors for the diseased model (10% perturbation) using Method I.

Different organs of the model	Complex dielectric in normal condition	Complex dielectric in diseased condition	Reconstructed complex dielectric with the proposed algorithm	Error found in the reconstructed values (%)
Fat	$25 - j5$	$25 - j5$	$25.20867 - j5.24254$	0.9920
Muscle	$50 - j23$	$50 - j23$	$50.36450 - j22.96961$	0.5791
Muscle Type	$35 - j15$	$35 - j15$	$35.22725 - j15.00306$	0.5519
Pancreas	$65 - j30$	$65 - j30$	$65.26897 - j30.01766$	0.3515
<b>Liver</b>	$46 - j10$	$41.4 - j9$	$41.59888 - j9.00577$	9.5845
Stomach	$60 - j18$	$60 - j18$	$60.23713 - j18.01148$	0.3678
Water	$76 - j40$	$76 - j40$	$76 - j40$	0.0000

**Table 11:** Analysis with negative perturbations of the reconstructed dielectrics and corresponding errors for the diseased model (15% perturbation) using Method I.

Different organs of the model	Complex dielectric in normal condition	Complex dielectric in diseased condition	Reconstructed complex dielectric with the proposed algorithm	Error found in the reconstructed values (%)
Fat	$25 - j5$	$25 - j5$	$25.20840 - j4.42036$	0.3841
Muscle	$50 - j23$	$50 - j23$	$50.10479 - j24.03536$	0.9723
Muscle Type	$35 - j15$	$35 - j15$	$35.28049 - j14.71091$	0.3828
Pancreas	$65 - j30$	$65 - j30$	$65.26733 - j30.01473$	0.3477
<b>Liver</b>	$46 - j10$	$39.1 - j8.5$	$39.20390 - j8.45233$	14.8057
Stomach	$60 - j18$	$60 - j18$	$60.06277 - j17.90934$	0.2364
Water	$76 - j40$	$76 - j40$	$76 - j40$	0.0000

**Table 12:** Analysis with negative perturbations of the reconstructed dielectrics and corresponding errors for the diseased model (20% perturbation) using Method I.

Different organs of the model	Complex dielectric in normal condition	Complex dielectric in diseased condition	Reconstructed complex dielectric with the proposed algorithm	Error found in the reconstructed values (%)
Fat	$25 - j5$	$25 - j5$	$25.34227 - j5.47021$	1.6898
Muscle	$50 - j23$	$50 - j23$	$50.95795 - j22.79272$	1.4295
Muscle Type	$35 - j15$	$35 - j15$	$35.43258 - j15.06917$	1.1161
Pancreas	$65 - j30$	$65 - j30$	$65.56699 - j30.04607$	0.7464
<b>Liver</b>	$46 - j10$	$36.8 - j8$	$37.24126 - j8.01716$	19.0761
Stomach	$60 - j18$	$60 - j18$	$60.71971 - j18.13100$	1.1606
Water	$76 - j40$	$76 - j40$	$76 - j40$	0.0000



**Table 13:** Analysis with negative perturbations of the reconstructed dielectrics and corresponding errors for the diseased model (mixed perturbation) using Method I.

Different organs of the model	Complex dielectric in normal condition	Complex dielectric in diseased condition	Reconstructed complex dielectric with the proposed algorithm	Error found in the reconstructed values (%)
Fat	$25 - j5$	$25 - j5$	$23.78462 - j6.68353$	3.0957
Muscle	$50 - j23$	$50 - j23$	$50.08430 - j26.04166$	2.5686
Muscle Type	$35 - j15$	$35 - j15$	$36.46439 - j15.66881$	4.2266
Pancreas	$65 - j30$	$65 - j30$	$65.22945 - j30.37229$	0.5094
Liver	$43.7 - j9.5$	$48.3 - j10.5$	$43.74286 - j9.49063$	4.9319
		$41.4 - j9$	$41.59888 - j9.00577$	9.5845
		$39.1 - j8.5$	$39.20390 - j8.45233$	14.8057
		$36.8 - j8$	$37.24126 - j8.01716$	19.0761
Stomach	$60 - j18$	$60 - j18$	$60.04776 - j18.32504$	0.2232
Water	$76 - j40$	$76 - j40$	$76 - j40$	0.0000

**Table 14:** Analysis with negative perturbations of the reconstructed dielectrics and corresponding errors for the diseased model (mixed perturbation) using Method II.

Different organs of the model	Complex dielectric in normal condition	Complex dielectric in diseased condition	Reconstructed complex dielectric with the proposed algorithm	Error found in the reconstructed values (%)
Liver	$46 - j10$	$43.7 - j9.5$	$43.70001 - j9.49999$	5.0001
		$41.4 - j9$	$41.39999 - j9.00001$	10.0000
		$39.1 - j8.5$	$39.10001 - j8.49999$	15.0002
		$36.8 - j8$	$36.800001 - j8.00002$	20.0001

**Table 15:** Comparison between the errors found using Method I and II with negative perturbations in the affected liver region.

Different organs of the model	Complex dielectric in normal condition	Complex dielectric in diseased condition	Error found in the reconstructed values (%) using Method I	Error found in the reconstructed values (%) using Method II
Liver	$46 - j10$	$43.7 - j9.5$	4.9319	5.0001
		$41.4 - j9$	9.5845	10.0000
		$39.1 - j8.5$	14.8057	15.0002
		$36.8 - j8$	19.0761	20.0001

**Table 16:** Analysis using mixed perturbation (5% and 15% positive perturbation and 10% and 20% negative perturbation).

Perturbation rate of the complex dielectric	Complex dielectric in normal condition	Perturbed complex dielectric in diseased condition
5%	$46 - j10$	$48.3 - j10.5$
10%	$46 - j10$	$41.4 - j9$
15%	$46 - j10$	$52.9 - j11.5$
20%	$46 - j10$	$36.8 - j8$

### 6.3 Data Analysis with a Combination of Positive and Negative Perturbations in the Complex Dielectric

In this section, a further extension of the algorithm is constructed. The complex permittivity of some

cells in the affected liver region are considered to be positively perturbed while others are negatively perturbed. Tables 16–18 present tabular analyses, demonstrating that the algorithm is also efficient in segregating normal and affected dielectrics with minimum errors in this type of mixed situation.

## 7. RESULTS EVALUATION

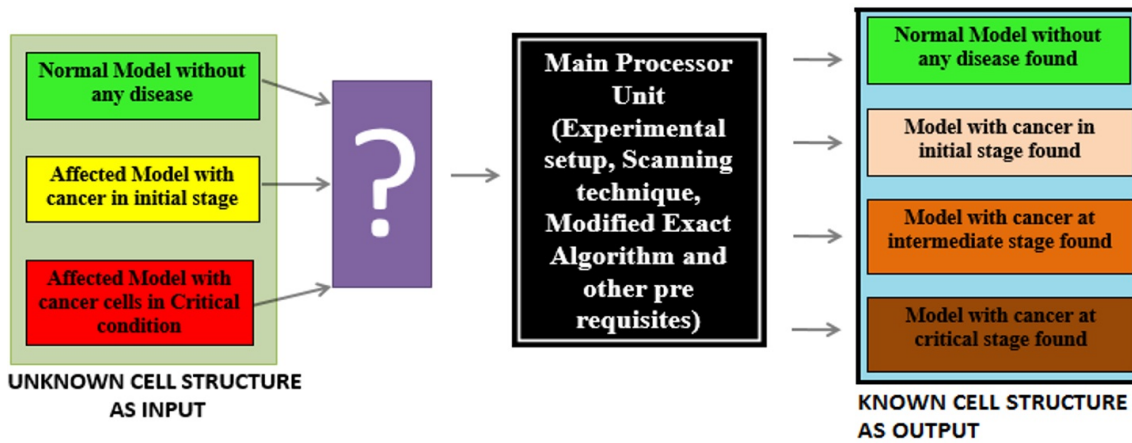
From the above-mentioned tabular analysis, it has been shown clearly that the newly defined modified exact reconstruction algorithm works nicely on all possible kinds of deviations of complex dielectrics in a cancer-affected biological target. Table 2 shows the mathematical data output of the experiment where the complex dielectric of the water content of the affected liver region is perturbed by 5% in the positive direction with respect to its standard normal value. The fifth column shows that using Method I, the

**Table 17:** Analysis with a combination of positive and negative perturbations of the reconstructed dielectrics and corresponding errors for the diseased model (mixed perturbation) using Method II.

Different organs of the model	Complex dielectric in normal condition	Complex dielectric in diseased condition	Reconstructed complex dielectric with the proposed algorithm	Error found in the reconstructed values (%)
<b>Liver</b>	$46 - j10$	$48.3 - j10.5$	$48.89481 - j10.44295$	6.336626
		$41.4 - j9$	$41.95843 - j9.01618$	8.833240
		$52.9 - j11.5$	$53.37144 - j11.58834$	16.087463
		$36.8 - j8$	$36.81822 - j14.45639$	18.841673

**Table 18:** Analysis with a combination of positive and negative perturbations of the reconstructed dielectrics and corresponding errors for the diseased model (mixed perturbation) using Method II.

Different organs of the model	Complex dielectric in normal condition	Complex dielectric in diseased condition	Reconstructed complex dielectric with the proposed algorithm	Error found in the reconstructed values (%)
<b>Liver</b>	$46 - j10$	$48.3 - j10.5$	$48.30001 - j10.49999$	5.0001
		$41.4 - j9$	$41.400001 - j8.99999$	10.0000
		$52.9 - j11.5$	$52.89999 - j11.50000$	15.0001
		$36.8 - j8$	$36.79999 - j8.00001$	20.0000

**Fig. 4:** Summary of the overall workflow.

deviation is found to be 4.9289%, and Method II in Table 7 gives the exact value with no error. Likewise, 10%, 15%, and 20% perturbed conditions are also checked in the respected tables. Similar analysis has been conducted for negative complex dielectric deviations as well.

Tables 6 and 13 show additional important results, with a mixture of different dielectric conditions applied to the affected region, and the reconstruction algorithm using Methods I and II is also able to segregate the respective dielectric cells and their proper positions inside the body. Table 17 shows the cells of the affected region demonstrating peculiar behavior with the dielectric constant of some cells increasing while others decrease. Even in this kind of situation the proposed algorithm works effectively, generating the optimum results presented in their respective tables.

All possible combinations of dielectric constants may occur when a region inside the human body is affected by a cancerous tumor. Hence, this kind of algorithm is extremely effective due to its ability to adapt to deviations and provide proper results no matter what kind of behavior a particular cell may exhibit. These analyses prove the optimum impact of our proposed algorithm in the detection of cancer-affected cells inside the human body.

The overall workflow of this work presents in Fig. 4.

## 8. CONCLUSION AND FUTURE WORKS

Cancer treatment remains a critical issue for scientists, researchers, and doctors in the field of biomedical engineering. The abrupt and indeterministic behaviors of cancer cells make it difficult to cure especially during the later stages of the disease.

However, researchers throughout the globe are attempting to find possible solutions for curing cancer. Methodologies and techniques are continuously being improvised to reduce the major causality of this disease.

The main concept behind this study is to derive an algorithm with the potential to detect all types of behavior in a cancer-affected cell. With this in mind, a modified microwave tomography-based complex cell dielectric reconstruction algorithm has been developed in this work.

After examining all possible kinds of deviations in complex cell permittivity, the proposed technique has been found to work very well in all such conditions, producing minimum errors in every case. The newly framed modified reconstruction algorithm is very efficient in identifying even small dielectric perturbations in affected cells, and will also be helpful in the early detection of cancer. Method II produces almost 100% accuracy in all the cases. This fresh approach may provide a new dimension in the diagnosis of many other fatal diseases as well as cancer in the future. All the programs relating to field calculations, iterative reconstruction, model formation, complex dielectric calculations, etc., have been performed in this study using FORTRAN and C programming with Force 2.0 and CODEBLOCK software, respectively. All the graphical models have been simulated using MATLAB programming. In the future, we plan to check other important parameters relating to the output results to observe the effect of noise. It is also possible to produce an extended version of the modified algorithm capable of providing superior tolerance to noise. We will also extend this work in an attempt to apply the algorithm in real-life situations by creating an experimental setup with a proper transmitter and receiver and feeding this algorithm to check the results and compare them with the theoretically measured values for error calculation. The extended works in this field are expected to be intensively applied in the biomedical engineering field in the near future.

## ACKNOWLEDGMENT

We would like to thank the Associate Editor and all anonymous reviewers for their valuable comments and suggestions, which have helped us to improve our work. The previous version of this work was published in [32]. The work has been further modified and extended for submission to the journal. There is no point of conflict between the co-authors regarding the information and results presented in this work.

## REFERENCES

- [1] S. Hosseinzadegan, "Fast Microwave Tomography Algorithm for Breast Cancer Imaging," Ph.D. dissertation, Dept. Elect. Eng., Chalmers University of Technology, Göteborg, Sweden, 2021.
- [2] D. Kurrant, M. Omer, N. Abdollahi, P. Mojabi, E. Fear, and J. LoVetri, "Evaluating Performance of Microwave Image Reconstruction Algorithms: Extracting Tissue Types with Segmentation Using Machine Learning," *Journal of Imaging*, vol. 7, no. 1, 2021, Art. no. 5.
- [3] Y. Zhang, Y. Ma, A. Omrani, R. Yadav, M. Fjeld, and M. Fratarcangeli, "Automated Microwave Tomography (MWT) Image Segmentation: State-of-the-Art Implementation and Evaluation," *Computer Science Research Notes*, CSRN 3001, pp. 126–136, 2020.
- [4] E. R. Almeida, T. Bicudo, and J. L. Porsani, "Automatic estimation of inversion parameters for Microwave Tomography in GPR data using cooperative targets," *Journal of Applied Geophysics*, vol. 178, Jul. 2020, Art. no. 104074.
- [5] International Agency for Research on Cancer (IARC), "Latest global cancer data: Cancer burden rises to 18.1 million new cases and 9.6 million cancer deaths in 2018," World Health Organization, Lyon, France, Press Release No. 263, Sep. 12, 2018. [Online]. Available: <https://www.who.int/cancer/PRGlobocanFinal.pdf>
- [6] L. Wang, "Early Diagnosis of Breast Cancer," *Sensors*, vol. 17, no. 7, 2017, Art. no. 1572.
- [7] B. Sohani *et al.*, "Detection of haemorrhagic stroke in simulation and realistic 3-D human head phantom using microwave imaging," *Biomedical Signal Processing and Control*, vol. 61, 2020, Art. no. 102001.
- [8] T. Reimer, M. Solis-Nepote, and S. Pistorius, "The Application of an Iterative Structure to the Delay-and-Sum and the Delay-Multiply-and-Sum Beamformers in Breast Microwave Imaging," *Diagnostics*, vol. 10, no. 6, 2020, Art. no. 411.
- [9] A. K. Trull, J. van der Horst, L. J. van Vliet, and J. Kalkman, "Comparison of image reconstruction techniques for optical projection tomography," *Applied Optics*, vol. 57, no. 8, pp. 1874–1882, 2018.
- [10] A. K. Kundu, B. Bandyopadhyay, and S. Sanyal, "A Microwave Imaging and Enhancement Technique from Noisy Synthetic Data," *ANNALS of Faculty Engineering Hunedoara – International Journal of Engineering*, vol. 9, no. 1, pp. 175–178, 2011.
- [11] K. Purkait, D. Basu, and N. R. Das, "An Approach To A Narrow Beam Antenna For Microwave Scanning Of Stroke Affected Brain Cells," *Indian Science Cruiser*, vol. 32, no. 3, pp. 43–46, May 2018.
- [12] K. Purkait, D. Basu, and N. R. Das, "Study of Beamwidth Variation of Dipole Array Antenna for Microwave Scanning of Biological Target,"

- International Journal on Recent and Innovation Trends in Computing and Communication*, vol. 6, no. 1, pp. 120–123, Jan. 2018.
- [13] J. Richmond, "Scattering by a dielectric cylinder of arbitrary cross section shape," *IEEE Transactions on Antennas and Propagation*, vol. 13, no. 3, pp. 334–341, May 1965.
  - [14] A. N. Datta and D. B. Bandyopadhyay, "An Improved SIRT-Style Reconstruction Algorithm for Microwave Tomography," *IEEE Transactions on Biomedical Engineering*, vol. BME-32, no. 9, pp. 719–723, Sep. 1985.
  - [15] S. Mandal and K. Purkait, "A Modified Exact Reconstruction Algorithm for Microwave Tomography for Detection of Disease in Human Body," *International Journal of Tomography & Statistics*, vol. 18, no. F11, pp. 82–93, 2011.
  - [16] S. Saha, G. Pal, S. Pyne, and S. Mandal, "Tomography of Human Body using Exact Simultaneous Iterative Reconstruction Algorithm," *Computer Science & Information Technology*, vol. 3, no. 2, pp. 437–443, 2013.
  - [17] J. H. Jacobi, L. E. Larsen, and C. T. Hast, "Water-Immersed Microwave Antennas and Their Application to Microwave Interrogation of Biological Targets," *IEEE Transactions on Microwave Theory and Techniques*, vol. 27, no. 1, pp. 70–78, Jan. 1979.
  - [18] L. E. Larsen and J. H. Jacobi, "Microwave scattering parameter imagery of an isolated canine kidney," *Medical Physics*, vol. 6, no. 5, pp. 394–403, Sep. 1979.
  - [19] A. Joisel *et al.*, "Microwave imaging techniques for biomedical applications," in *Proceedings of the 16th IEEE Instrumentation and Measurement Technology Conference (IMTC/99)*, vol. 3, 1999, pp. 1591–1596.
  - [20] J. C. Bolomey, L. Jofre, and G. Peronnet, "On the Possible Use of Microwave-Active Imaging for Remote Thermal Sensing," *IEEE Transactions on Microwave Theory and Techniques*, vol. 31, no. 9, pp. 777–781, Sep. 1983.
  - [21] S. Y. Semenov *et al.*, "Microwave tomography: two-dimensional system for biological imaging," *IEEE Transactions on Biomedical Engineering*, vol. 43, no. 9, pp. 869–877, Sep. 1996.
  - [22] D. Li, P. M. Meaney, and K. D. Paulsen, "Conformal microwave imaging for breast cancer detection," *IEEE Transactions on Microwave Theory and Techniques*, vol. 51, no. 4, pp. 1179–1186, Apr. 2003.
  - [23] Q. Fang, P. M. Meaney, S. D. Geimer, A. V. Streltsov, and K. D. Paulsen, "Microwave image reconstruction from 3-D fields coupled to 2-D parameter estimation," *IEEE Transactions on Medical Imaging*, vol. 23, no. 4, pp. 475–484, Apr. 2004.
  - [24] E. J. Bond, X. Li, S. C. Hagness, and B. D. Van Veen, "Microwave imaging via space-time beamforming for early detection of breast cancer," *IEEE Transactions on Antennas and Propagation*, vol. 51, no. 8, pp. 1690–1705, Aug. 2003.
  - [25] W. C. Chew and Y. M. Wang, "Reconstruction of two-dimensional permittivity distribution using the distorted Born iterative method," *IEEE Transactions on Medical Imaging*, vol. 9, no. 2, pp. 218–225, Jun. 1990.
  - [26] S. Caorsi, G. L. Gagnani, and M. Pastorino, "Two-dimensional microwave imaging by a numerical inverse scattering solution," *IEEE Transactions on Microwave Theory and Techniques*, vol. 38, no. 8, pp. 981–989, Aug. 1990.
  - [27] C. Estatico, M. Pastorino, and A. Randazzo, "A Novel Microwave Imaging Approach Based on Regularization in  $L^p$  Banach Spaces," *IEEE Transactions on Antennas and Propagation*, vol. 60, no. 7, pp. 3373–3381, Jul. 2012.
  - [28] P. Lu, J. Córcoles, and P. Kosmas, "Non-linear Microwave Imaging Using Fast Iterative Shrinkage Thresholding," in *2019 Photonics & Electromagnetics Research Symposium - Spring (PIERS-Spring)*, 2019, pp. 1949–1956.
  - [29] M. Hopfer, R. Planas, A. Hamidipour, T. Henriksson, and S. Semenov, "Electromagnetic Tomography for Detection, Differentiation, and Monitoring of Brain Stroke: A Virtual Data and Human Head Phantom Study," *IEEE Antennas and Propagation Magazine*, vol. 59, no. 5, pp. 86–97, Oct. 2017.
  - [30] A. Goetzke-Pala, A. Hoła, and Ł. Sadowski, "A non-destructive method of the evaluation of the moisture in saline brick walls using artificial neural networks," *Archives of Civil and Mechanical Engineering*, vol. 18, no. 4, pp. 1729–1742, Sep. 2018.
  - [31] Z. Wu and H. Wang, "Microwave Tomography for Industrial Process Imaging: Example Applications and Experimental Results," *IEEE Antennas and Propagation Magazine*, vol. 59, no. 5, pp. 61–71, Oct. 2017.
  - [32] D. Basu and K. Purkait, "A Hypothetical Analysis to Study the Variations of Complex Dielectric Permittivity for Detection of Various Stages of Cancer of a Biological Target using Microwave Tomography," in *2019 Devices for Integrated Circuit (DevIC)*, 2019, pp. 433–440.
  - [33] Z. Vilagosh, A. Lajevardipour, D. Appadoo, S. Juodkazis, and A. W. Wood, "Using Attenuated Total Reflection (ATR) Apparatus to Investigate the Temperature Dependent Dielectric Properties of Water, Ice, and Tissue-Representative Fats," *Applied Sciences*, vol. 11, no. 6, 2021, Art. no. 2544.
  - [34] T. Saito, H. Asano, H. Saito, R. Kita, N.

- Shinyashiki, and S. Yagihara, "Effects of Blood Stream on Non-Invasive Dielectric Spectroscopy Measurements for Biological Tissues," *Transactions of the Materials Research Society of Japan*, vol. 45, no. 4, pp. 149–152, 2020.
- [35] D. A. Pollacco, L. Farina, P. S. Wismayer, L. Farrugia, and C. V. Sammut, "Characterization of the dielectric properties of biological tissues and their correlation to tissue hydration," *IEEE Transactions on Dielectrics and Electrical Insulation*, vol. 25, no. 6, pp. 2191–2197, Dec. 2018.
- [36] X. Li, F. Yang, and B. Rubinsky, "A Correlation Between Electric Fields That Target the Cell Membrane Potential and Dividing HeLa Cancer Cell Growth Inhibition," *IEEE Transactions on Biomedical Engineering*, vol. 68, no. 6, pp. 1951–1956, Jun. 2021.
- [37] K. Zhu, N. R. Hum, B. Reid, Q. Sun, G. G. Loots, and M. Zhao, "Electric Fields at Breast Cancer and Cancer Cell Collective Galvanotaxis," *Scientific Reports*, vol. 10, no. 1, 2020, Art. no. 8712.
- [38] Y. Zhou, D. Yang, Y. Zhou, B. L. Khoo, J. Han, and Y. Ai, "Characterizing Deformability and Electrical Impedance of Cancer Cells in a Microfluidic Device," *Analytical Chemistry*, vol. 90, no. 1, pp. 912–919, 2018.
- [39] A. Gupta and G. U. Kharat, "Modeling of Dielectric Properties of Cancer Cell and Evaluation of Cancer Stages: A Review," *International Journal of Recent Scientific Research*, vol. 5, no. 2, pp. 443–448, Feb. 2014.
- [40] Z. Wei and X. Chen, "Induced-Current Learning Method for Nonlinear Reconstructions in Electrical Impedance Tomography," *IEEE Transactions on Medical Imaging*, vol. 39, no. 5, pp. 1326–1334, May 2020.
- [41] D. Basu and K. Purkait, "Dynamic Nature of Electric Field Variations with Changing Dielectric Constant of Propagating Medium," *Journal of Electrical Engineering, Electronics, Control and Computer Science*, vol. 6, no. 9, pp. 1–6, 2020.
- [42] D. Basu and K. Purkait, "Analysis of Narrow Beamwidth Microwave Scanning Techniques of Biological Targets Using Dipole Array Antenna," in *Intelligent Techniques and Applications in Science and Technology* (Learning and Analytics in Intelligent Systems, vol. 12), S. Dawn, V. Balas, A. Esposito, and S. Gope, Eds. Cham, Switzerland: Springer Nature, 2020, pp. 383–393.



**Deborsi Basu** received his B.Tech degree in Electronics and Communication Engineering from Heritage Institute of Technology, Kolkata, West Bengal, India in 2016 and M.Tech degree in Communication Engineering from Kalyani Government Engineering College, Kalyani, West Bengal, India in 2018. He was the University Topper in the Specialization area of Communication Engineering in M.Tech. He is currently pursuing a Ph.D. degree from G. S. Sanyal School of Telecommunications, IIT Kharagpur with the joint collaboration of Vanderbilt University, Nashville, Tennessee, USA. His current research interest includes Software Defined Networking (SDN), OpenFlow Protocol Design, Network Function Virtualization (NFV), Federated Cloud & Edge Computing in 5G and beyond Communication Networks. He has authored papers in reputed flagship conferences, magazines and journals which include IEEE WCNC, IEEE GlobeCom, IEEE INFOCOM, ACM MobiCom, IEEE Transactions, Elsevier, Springer, etc. He is the recipient of multiple prestigious conference and travel grant awards from IEEE ComSoc, ACM SIGCOM, and other organizations. He has also received multiple best conference and poster awards from international and national level conferences that include IEEE GCAIoT, ICIMSAT Springer, Mindshare YUVA, IEEE CS BDC Summer Symposium, etc. He is also serving as a project associate in communication standard development and regulatory bodies.



**Kabita Purkait** received her B.Tech in Radiophysics and Electronics from University of Calcutta, West Bengal, India in 1989, and her M.Tech in Radiophysics and Electronics from Calcutta University, West Bengal, India, in 1991. She has got CSIR fellowship as Senior Research Fellow and performed research work on Microwave Tomography in Rajabazar Science College campus of Calcutta University, West Bengal, India. In 1999 she joined as a Lecturer in the Department of Electronics & Telecommunication Engineering of Jnan Chandra Ghosh Polytechnic, West Bengal, India. She was awarded Ph.D. (Tech) from Calcutta University in 2006.

In 2008, Dr. Purkait has appointed as an Assistant Professor in the Department of Electronics and Communication Engineering in Kalyani Government Engineering College (KGEC), West Bengal, India. Currently, she is working as an Associate Professor in KGEC. Her present interest is in the development of a microwave scanner and subsequent reconstruction algorithm in Microwave Tomography.